Supplementary information

Direct synthesis of ultralight, elastic, high-temperature insulation N-doped TiO_2 ceramic nanofibrous sponges via electrospinning

Wei Cheng[1], Wenling Jiao[1]*, Yifan Fei[1], Zaihui Yang[1], Xiaohua Zhang[1], Fan Wu[1], Yitao Liu[1], Xia Yin[1]* and Bin Ding[1]

[1] Key Laboratory of Textile Science & Technology (Ministry of Education), College of Textiles and Innovation Center for Textile Science and Technology, Donghua University, Shanghai 201620, China

* Correspondence: wenlingjiao@dhu.edu.cn, xyin@dhu.edu.cn

Supplementary Movies

Movie S1 Spinning and stacking processes

Movie S2 Dynamic compression recovery process

Movie S3 Burning process of N-TiO_2 CNSs at alcohol blowtorch

Supplementary Figures

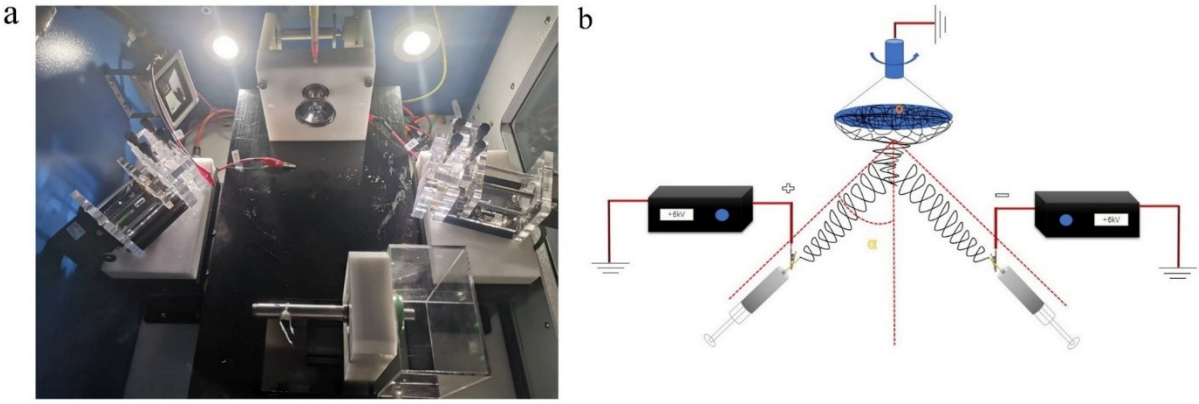

Figure S1. Schematic diagram of conjugate electrospinning. (a) A physical picture. (b) A mechanism image

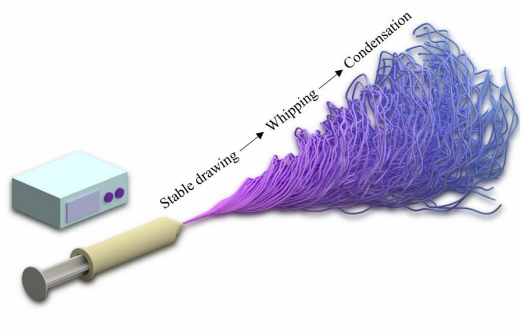

Figure S2. Different regions of the Taylor cone in electrospinning

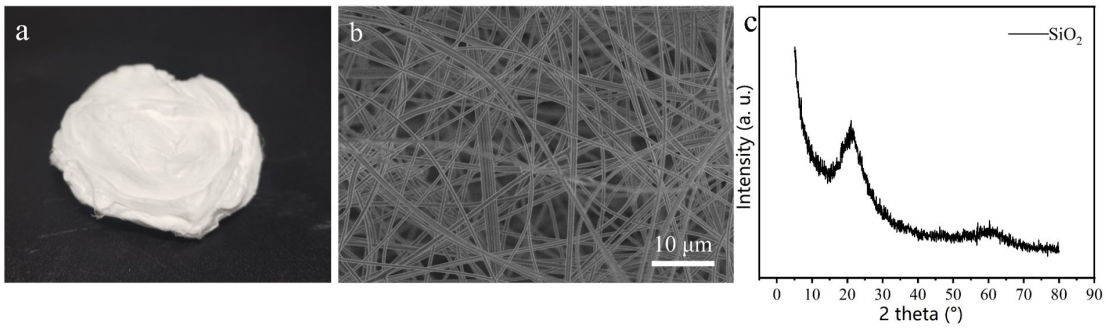

Figure S3. Structural characterization of SiO_2 nanofibrous sponges. (a) Physical picture of a SiO_2 nanofibrous sponge. (b) SEM image of SiO_2 nanofibers. (c) XRD data of SiO_2 nanofibers.

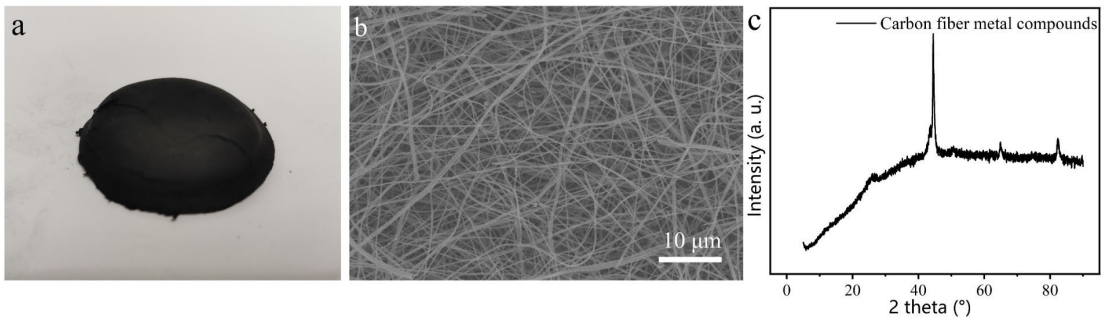

Figure S4. Structural characterization of carbon fiber metal compounds nanofibrous sponges. (a) Physical picture of a carbon nanofibrous sponge (b) SEM image of carbon nanofibers. (c) XRD data of carbon nanofibers

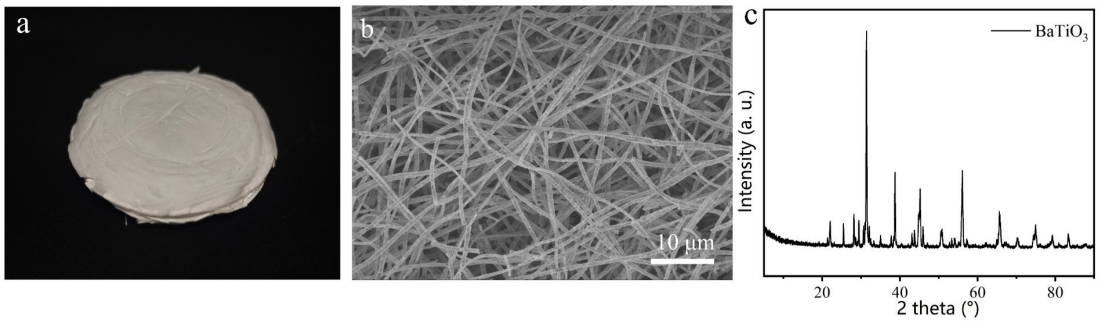

Figure S5. Structural characterization of $TiBaO_3$ nanofibrous sponges. (a) Physical picture of a $TiBaO_3$ nanofibrous sponge (b) SEM image of $TiBaO_3$ nanofibers. (c) XRD data of $TiBaO_3$ nanofibers.

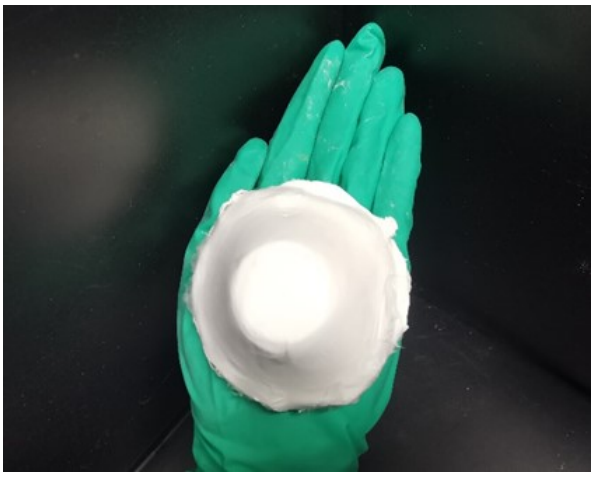

Figure S6. The precursor of N-TiO_2 CNSs with a diameter of 7.5 cm and a thickness of 3.5 cm.

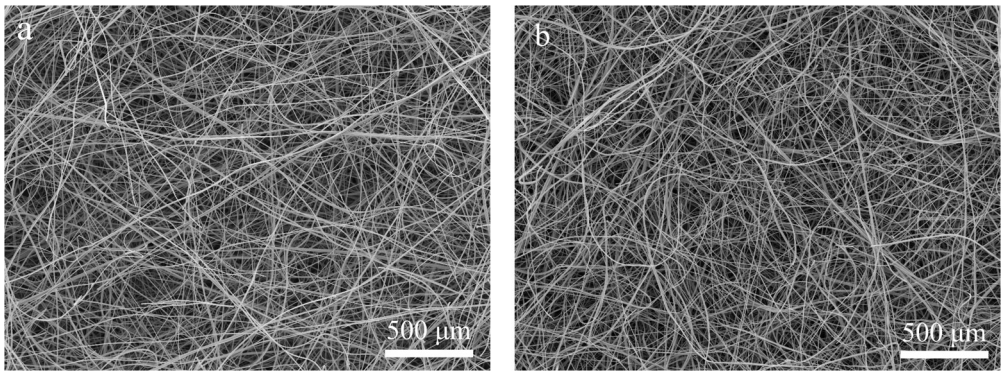

Figure S7. (a) SEM image of the surface lamellar of N-TiO_2 CNSs. (b) SEM image of the inner layer of N-TiO_2 CNSs.

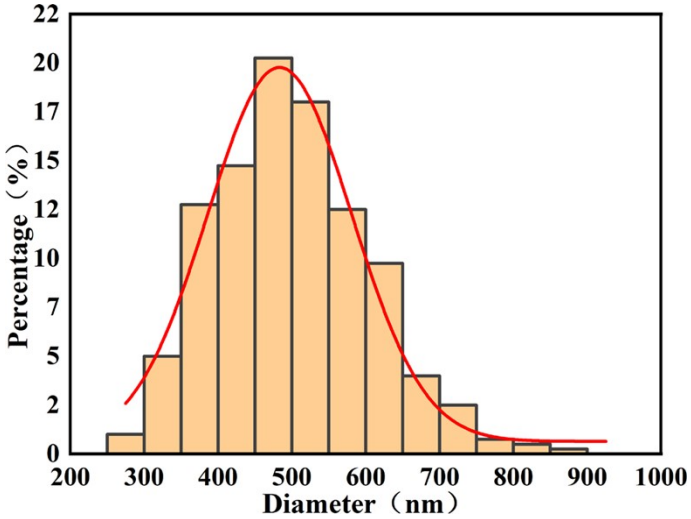

Figure S8. The fiber diameter distribution in the surface layer of the sponge.

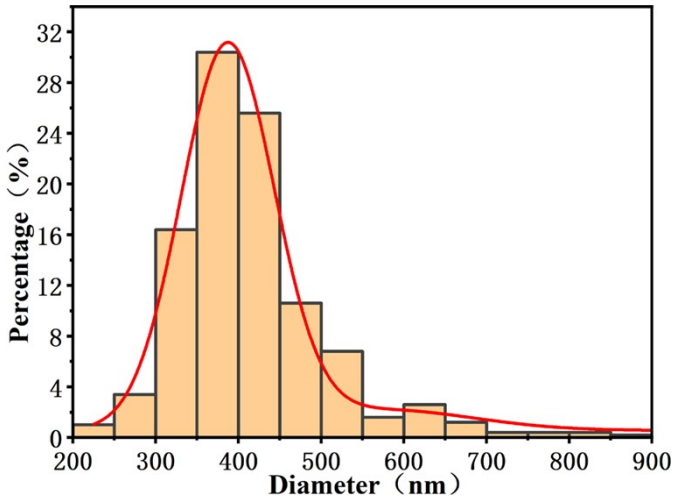

Figure S9. The fiber diameter distribution of the inner layer of the sponge.

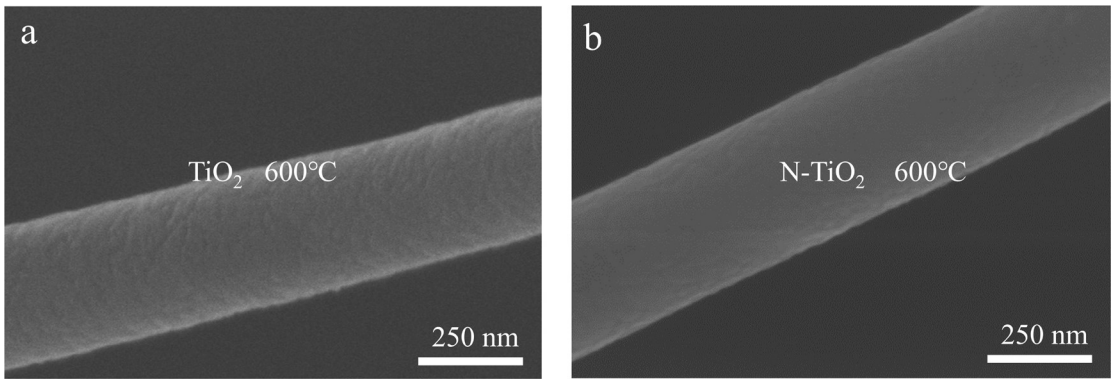

Figure S10. SEM images of TiO_2 and N-TiO_2 nanofibers after calcination at 600 ℃ for 1h.

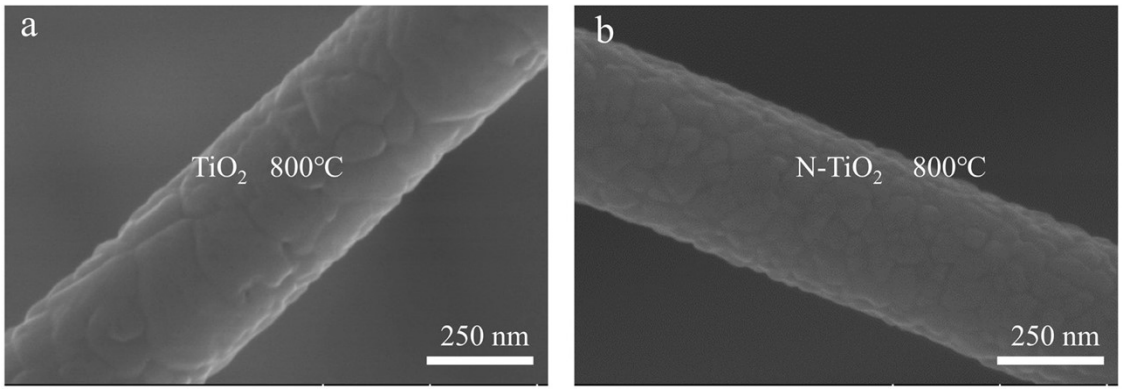

Figure S11. SEM images of TiO_2 and N-TiO_2 nanofibers after calcination at 800 ℃ for 1h.

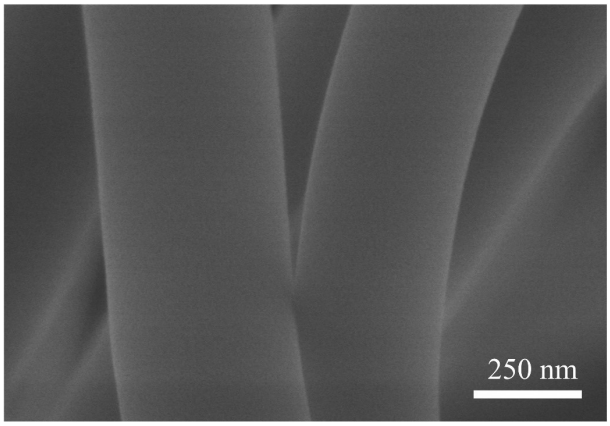

Figure S12. SEM image of bonding points between N-TiO_2 nanofibers

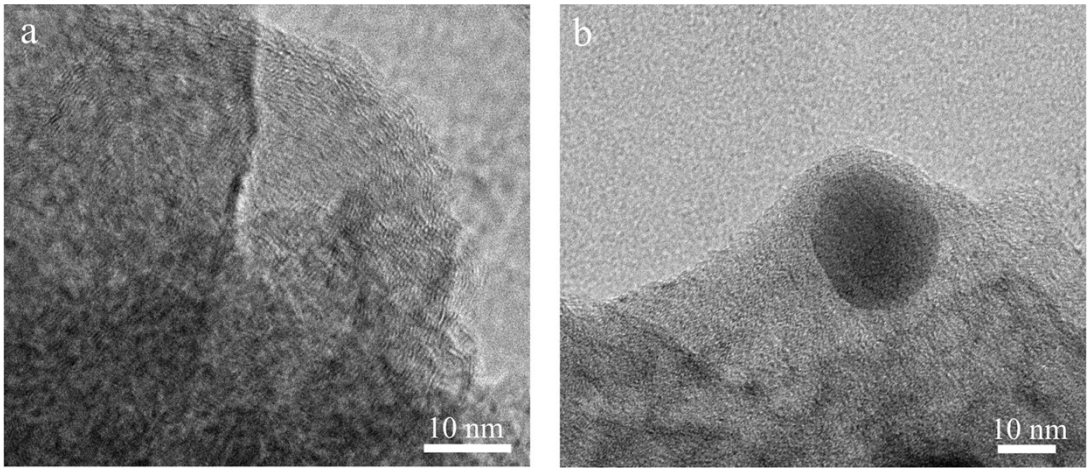

Figure S13. TEM images at the fracture site of N-TiO_2 nanofiber.

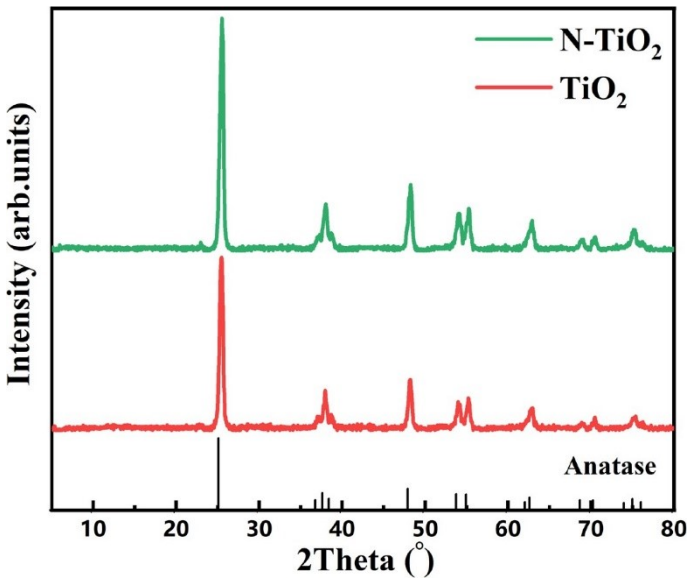

Figure S14. XRD spectra of TiO_2 and N-TiO_2 CNSs.

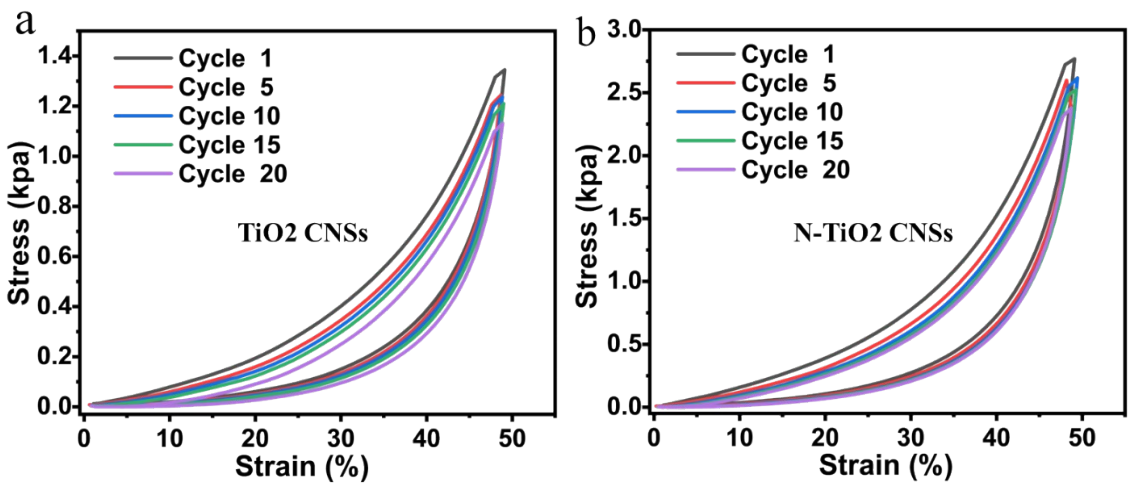

Figure S15. Compression resilience test results of TiO_2 CNSs and N-TiO_2 CNSs with a density of about 15 mg cm^{-3}. (a) TiO_2 CNSs. (b) N-TiO_2 CNSs.

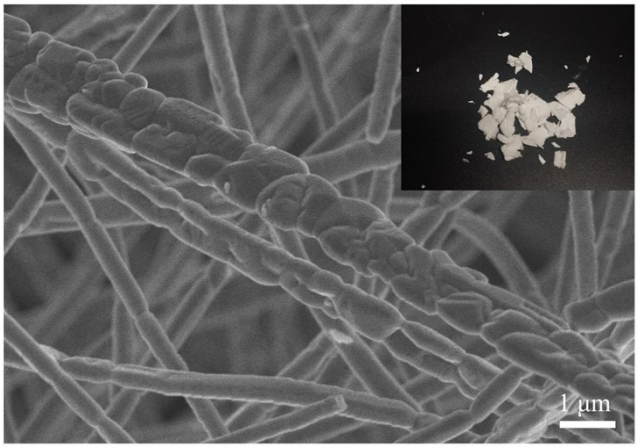

Figure S16. SEM image of N-TiO_2 after calcination at 1000 ° C for 1h, the inset is a physical picture.

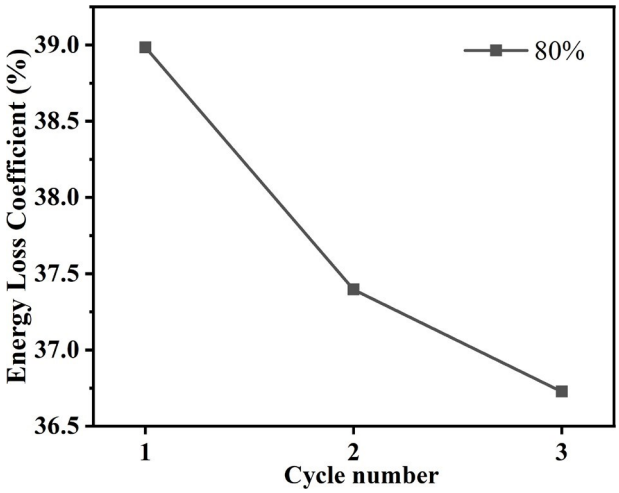

Figure S17. Energy loss coefficient of 12 mg cm^{-3} N-TiO_2 CNSs at 80% strain.

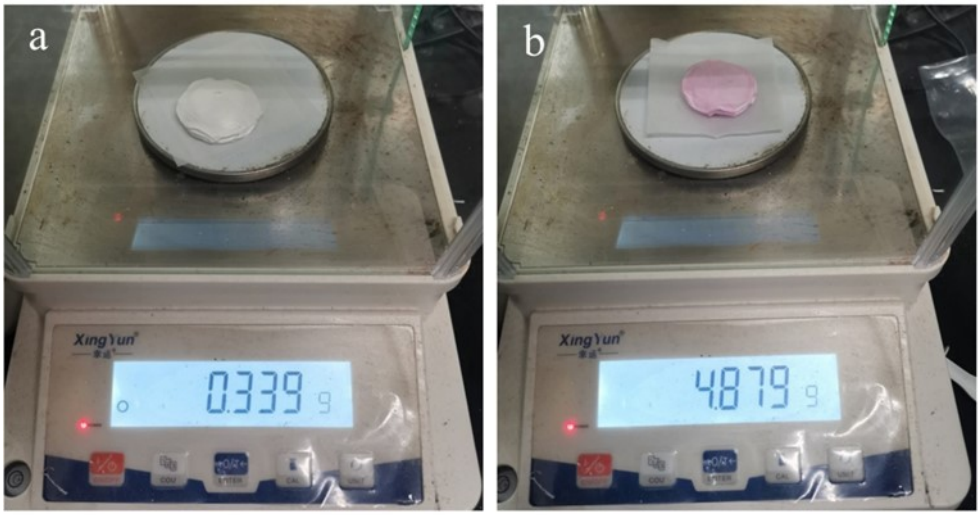

Figure S18. Hydroscopicity of TiO_2 nanofibrous sponge.

Supplementary Tables

Table S1. Automatic fast surface and porosity tests results

BJH Pore Size Distribution Adsorption	Surface Area(m^2 g^{-1})	Pore volume(cc g^{-1})
N-TiO_2	14.258	0.038
TiO_2	16.806	0.045
BJH Pore Size Distribution Desorption	**Surface Area(m^2 g^{-1})**	**Pore volume(cc g^{-1})**
N-TiO_2	36.946	0.049
TiO_2	39.506	0.054